Novel embedded Pd@CeO_2 catalysts: a way to active and stable catalysts†

Matteo Cargnello,[a] Tiziano Montini,[a] Stefano Polizzi,[b] Noah L. Wieder,[c] Raymond J. Gorte,[c] Mauro Graziani[a] and Paolo Fornasiero*[a]

Received 5th August 2009, Accepted 16th November 2009
First published as an Advance Article on the web 23rd December 2009
DOI: 10.1039/b916035c

1-wt% Pd-CeO_2 catalysts were prepared by co-precipitation of Pd nanoparticles with ceria (Pd@CeO_2-CP), by a microemulsion procedure (Pd@CeO_2-ME), and by normal impregnation of Pd salts (Pd/CeO_2-IMP) in order to test the concept that Pd-CeO_2 catalysts could be more stable for the water-gas-shift (WGS) reaction when the Pd is embedded in CeO_2. Initial WGS rates measured at 250 °C were similar for the Pd@CeO_2-CP and Pd/CeO_2-IMP, indicating that Pd was accessible for gas-phase reactions on both catalysts. Pd@CeO_2-CP exhibited better stability for WGS than did Pd/CeO_2-IMP but exposure to the WGS environment at 400 °C still caused a decrease in activity. Physical characterization of the Pd@CeO_2-ME implied that the core-shell nanoparticles underwent condensation that resulted in a low surface area and poor Pd accessibility. However, the Pd@CeO_2-ME sample exhibited good stability for WGS, suggesting that more effective encapsulation of Pd can limit the sintering of the metal phase, thus resulting in stable catalysts under high temperature reaction conditions.

1. Introduction

There has been significant progress recently in the preparation of nanometre-sized, metal particles that have well-defined shapes and sizes. This has been accomplished by manipulating the appropriate precursors on the atomic scale, typically using organic capping agents as protective layers.[1,2] The approach has also been used to synthesize materials with interesting catalytic properties, having both metal and oxide components.[3]

For catalytic applications, a major problem is the tendency of the active metal phase to sinter into larger particles. The loss of active surface area associated with particle growth often leads to poor long-term stability. The usual solution to this problem involves producing a barrier layer over the metal particles to prevent them from coming into contact with each other. For liquid-phase reactions performed at room temperature (RT), this barrier can be the organic capping molecules;[4,5] however, the use of organic molecules as a barrier fails with medium- and high-temperature reactions due to the fact that organic capping molecules generally decompose above 300 °C.

Barrier layers with improved thermal stability can be produced from oxides.[6] For this reason, "core-shell" catalysts composed of metal nanoparticles surrounded by metal-oxide shells have been prepared. Most of the work in this area has used SiO_2 as the oxide shell that covers the metal core, primarily because silicon alkoxides are readily available and easy to work with. As an example of work in this area, Joo, *et al.*[7] were able to prepare Pt nanoparticles encapsulated in mesoporous SiO_2 and then to show that the Pt particles were stable against calcination in air at 750 °C. Similarly, Park, *et al.*[8] prepared Pd particles inside a SiO_2 shell and then demonstrated that this catalyst remained active and stable for CO oxidation and ethylene hydrogenation. Some other examples dealt with the use of different oxide shells, such as ZrO_2 in the case of the preparation of Au particles entrapped into hollow spheres made up by a thin layer of zirconia.[9]

Attempts have also been made to produce core-shell catalysts in which the oxide shell is itself a promoter for catalytic activity. For example, CeO_2 is an important support for metal catalysts due to its ability to transfer lattice oxygen to metals in contact with it and therefore to promote reactions assisted by oxygen transfer. Ceria is particularly effective at promoting reactions in which steam is the oxidant, such as with the Water-Gas-Shift Reaction (WGS).[10] Because nanocrystalline forms of ceria are more reducible and more able to transfer oxygen,[11] core-shell materials based on ceria are especially promising. Indeed, Yeung, *et al.*[12,13] prepared Pt@CeO_2 catalysts and reported they were highly active for WGS under real reformate conditions, without producing CH_4 as a side product. It should be noted that Yeung *et al.* used a high Pt loading (5 wt%) and explained the high activity of their samples as resulting from CeO_2 that was electronically promoted by the buried metal particles. Moreover, the focus of their studies was on the activity of their samples rather than on long-term stability.

While ceria-supported precious metals have received significant attention for their high WGS activities, the long-term stability of these catalysts is a problem. For traditional ceria-supported Pt and Pd, it has been shown that the activity correlates with metal dispersion.[14] Unfortunately, the metal particles undergo significant sintering in the WGS environment, leading to loss of metal dispersion.[14,15] This problem must be resolved for them to be commercialized.

[a]*Chemistry Department, ICCOM-CNR Trieste Research Unit, Centre of Excellence for Nanostructured Materials (CENMAT) and INSTM Trieste Research Unit, University of Trieste, Via L. Giorgieri 1, 34127, Trieste, Italy*
[b]*Department of Physical Chemistry, University of Venice, INSTM Venice Research Unit, via Torino 155, 30172, Mestre, Venice, Italy*
[c]*Department of Chemical and Biomolecular Engineering, University of Pennsylvania, 311A Towne Building, 220 S. 33rd Street, Philadelphia, PA, 19104, USA*

† Work first presented at the 10th FIGIPAS Meeting in Inorganic Chemistry, Palermo, July 1–4, 2009.

In this paper, we report on the preparation of $Pd@CeO_2$ catalysts, using a microemulsion approach, with the goal of achieving active and stable WGS catalysts. The materials exhibit enhanced stability over traditional CeO_2-supported Pd catalysts but require optimization to enhance their catalytic activity.

2. Experimental

Pd-ceria catalysts were prepared in three different ways for this study: 1) Using polyvinylpyrrolidone (PVP)-protected Pd particles with coprecipitation of ceria; 2) using a microemulsion approach; and 3) using classical impregnation of preformed ceria. These samples are designated as $Pd@CeO_2$-CP, $Pd@CeO_2$-ME and Pd/CeO_2-IMP, respectively; and all were prepared with 1 wt% Pd. The solvents and materials in the various syntheses were used as received without further purification, with the exception that the solvents used in the synthesis of cerium alkoxide were dried over a 3-Å molecular sieve for at least 12 h prior to use.

2.1 Synthesis of $Pd@CeO_2$-CP

First, H_2O-soluble Pd nanoparticles were prepared using polyvinylpyrrolidone (PVP) as capping agent, following a procedure reported in the literature.[16] Briefly, H_2PdCl_4 was prepared by reacting 0.0887 g of $PdCl_2$ with 0.1 mL of concentrated HCl. The H_2PdCl_4 and 0.8325 g of PVP were then added to 150 mL of a 1/1 methanol–H_2O solution. Next, NaOH was added to the solution until the pH reached a value of 12 (final concentration of NaOH about 0.01 M). After the resulting solution was heated under reflux for 3 h in order to reduce Pd(II) to Pd(0) by means of methanol, it was gently cooled to room temperature. Finally, the solvents were evaporated, yielding a black solid which was used without further purification. In order to prevent any further oxidation of the metal, the Pd(0) nanoparticles were immediately used for the next co-precipitation step.

The $Pd@CeO_2$-CP was prepared by co-precipitation of the Pd nanoparticles together with ceria. Pd particles were first acidified until pH ~5 by means of conc. HNO_3. Following the addition of an aqueous solution (100 mL) of the acidified Pd nanoparticles and $Ce(NO_3)_3{\cdot}5H_2O$ to 200 mL of a 10% NH_4OH solution, with stirring, a pink gelatinous precipitate was immediately observed. After the precipitation was complete, 30 mL of a 10% H_2O_2 solution were added to the solution, dropwise, in order to enhance the catalyst texture.[17] The precipitate was aged under vigorous stirring for 1 h, then filtered and washed. The solid was then redispersed into 330 mL of isopropanol and left under reflux for 5 h to stabilize the porous structure of the material. The solid was again filtered, washed with isopropanol, and dried at 120 °C overnight. Finally, the solid was ground to achieve particle sizes smaller than 180 μm and calcined in air at 600 °C using a heating ramp of 3 °C min^{-1}.

2.2 Synthesis of $Pd@CeO_2$-ME

For this preparation, ceric tetrakis(octyloxide) was synthesized using a procedure that was slightly modified from that reported in the literature.[18,19] First, 7.8065 g of $(NH_4)_2Ce(NO_3)_6$ were dissolved into 40 mL of MeOH. Next, 9.00 mL of 1-octanol were added under vigorous stirring at room temperature. Then, a 25-wt% solution of MeONa in MeOH (19.54 mL) was added dropwise. Immediately, gaseous NH_3 and a bright yellow precipitate (probably $Ce(OCH_3)_4$) were formed. After the solvent was removed, the solid was suspended in 80 mL of toluene. This mixture was heated at 55 °C for 2 h, after which the MeOH formed in the reaction was evaporated. The mixture was stirred again at 55 °C for 2 h, then overnight at room temperature. Next, the solvents were partially removed and $NaNO_3$ filtered off before washing the product with toluene. The resulting orange solution was then rotary evaporated, leading to an oil with a deep orange color (8.7153 g, 93%). The ^{1}H-NMR spectrum of this oil was in accordance with literature data demonstrating that ceric tetrakis(octyloxide) had been formed.[18]

The $Pd@CeO_2$-ME catalyst was then prepared using a microemulsion approach. 33.45 mg of $Pd(NO_3)_2$ were dissolved into 10 mL of H_2O, while cetyltrimethylammonium bromide (CTAB, 15.7079 g) and n-butanol (14.55 mL, 11.79 g) were dissolved into 18 mL of isooctane. The aqueous solution containing Pd(II) was added to the organic solution of CTAB and n-butanol. The microemulsion composition (wt%) of CTAB-butanol/isooctane/H_2O was 55/25/20, while the total mass of the microemulsion was 50 g. After a few minutes, a clear yellow microemulsion was formed. N_2H_4 (21 μL, 3 mol *vs.* Pd) was used as reducing agent and added directly into the microemulsion, causing it to turn light brown initially, then later a deep brown with a large production of foam. This indicated the successful reduction of Pd(II) to Pd(0) in the aqueous droplets of the microemulsion, with Pd(0) nanoparticles protected by the surfactant molecules. After stirring for 1 h, 1.92 g of ceric tetrakis(octyloxide), dissolved in 2.5 mL of isooctane, were added dropwise to the microemulsion, causing the formation of orange flakes. After stirring for 2 h, isopropanol was added to break the microemulsion. The mixture was filtered and washed with isopropanol and H_2O in order to remove all the unbound surfactant, and then dried at 120 °C overnight. Finally, the solid was ground to achieve particle sizes smaller than 180 μm and calcined in air at 600 °C using a heating ramp of 3 °C min^{-1}. The calcination temperature and time ensured the complete removal of the organic residues from the synthesis (as verified by TPO-MS experiments and IR data).

2.3 Synthesis of Pd/CeO_2-IMP

A reference catalyst was prepared by incipient-wetness impregnation of a preformed ceria. The ceria used for this sample was produced using the same co-precipitation procedure described above, except that there was no H_2PdCl_4. After calcination at 600 °C for 5 h, the support was impregnated with the appropriate volume of an aqueous solution of $Pd(NO_3)_2{\cdot}2H_2O$ in order to obtain a metal loading of 1 wt%. After drying at 120 °C overnight, the sample was calcined at 400 °C for 5 h. No pre-activation/reduction step was applied before catalytic testing, as *in situ* reduction occurs under reaction conditions (see next section).

2.4 Catalytic and characterization techniques

All catalytic tests were conducted at atmospheric pressure.

The fresh catalysts were pretreated in a flowing mixture of 5% O_2–95% Ar at 40 mL min^{-1} for 30 min at 450 °C, after heating from room temperature at 10 °C min^{-1}. No other activation procedures (*e.g.* reduction) were necessary since the catalyst was reduced *in situ* under the WGS reaction conditions employed. Typically ~ 43 mg of

fresh sample were positioned in a U-shaped, quartz microreactor with internal diameter of 4 mm. The total gas flow rate under reaction conditions was 54.3 mL min^{-1} in order to ensure a Gas Hourly Space Velocity (GHSV) of ~75,000 mL g^{-1} h^{-1}. The feed gas for the WGS reaction was 3.0 vol% CO and 3.0 vol% H_2O, diluted in Ar. This gaseous mixture was introduced into the reactor at 250 °C for 2 h. Aging treatments were performed by heating the sample in the WGS environment at temperatures up to 400 °C and keeping it at this temperature for different time periods, as detailed. After that, the sample was cooled down to 250 °C in the WGS environment and the activity measured again. All heating and cooling rates were 2 °C min^{-1}. Reactants and products were analysed using a mass spectrometer (Hyden Analytical HPR20).

N_2 physisorption and H_2 chemisorption experiments were carried out on a Micromeritics ASAP 2020C. The samples were first degassed in vacuum at 350 °C overnight prior to N_2 adsorption at –195 °C. For H_2 chemisorption, the samples were placed in a U-shaped quartz reactor, heated in flowing 5% O_2–95% Ar and reduced in flowing 5% H_2-95% Ar at the desired temperatures, and then evacuated at 400 °C for 4 h. Hydrogen adsorption experiments were conducted at –90 °C by means of a solid-liquid acetone bath and in the pressure range from 1 to 20 Torr. Adsorption values were obtained by linear extrapolation to zero pressure.

Powder X-ray diffraction patterns were collected on a Philips PW 1710/01 instrument with Cu K_α radiation (graphite monochromator). Diffraction patterns were taken with a 0.02 degree step size, using a counting time of 10 s per point.

Before each temperature programmed reduction (TPR) experiment, the samples were pretreated in flowing 5% O_2-95% Ar mixtures at 450 °C. The measurements were performed in a conventional system equipped with a thermal conductivity detector (TCD),[20] under 5% H_2–95% Ar mixtures, using a gas flow rate of 25 mL min^{-1} and a heating rate 10 °C min^{-1}.

Samples for transmission electron microscopy (TEM) were prepared by placing a single drop of a sample dispersed in isopropanol onto a 200-mesh copper grid coated with an amorphous holey carbon film. The grid was then dried in air for 24 h. Images were obtained with a JEOL 3010 high-resolution electron microscope (1.7 nm point-to-point resolution), operating at 300 keV, using a Gatan slow-scan CCD camera (mod. 794). In order to identify Pd crystallites within the catalysts, microanalysis was made by using an Oxford Instruments Energy Dispersive X-Ray (EDX) spectrometer (mod. 6636) using a spot size of 25 nm.

3. Results and discussion

A summary of the physical properties of the Pd-ceria and the ceria samples examined in this study is given in Table 1. For each sample, the XRD patterns were those expected for a solid having a cubic fluorite structure. No reflections related to the Pd or PdO phases could be observed on the Pd-ceria samples due to the very low metal loadings. The average crystallite dimensions of the CeO_2 phase, calculated applying Scherrer's equation to the (111) reflection, were slightly smaller for the Pd@CeO_2-CP sample than for the other samples; however, it is not clear whether this difference is significant.

Textural differences in the four samples were readily apparent from the N_2 adsorption isotherms, shown in Fig. 1 and summarised in Table 1. All the samples show type IV isotherms typical of mesoporous materials, but the shape of the isotherms and the hysteresis depended strongly on the preparation method.

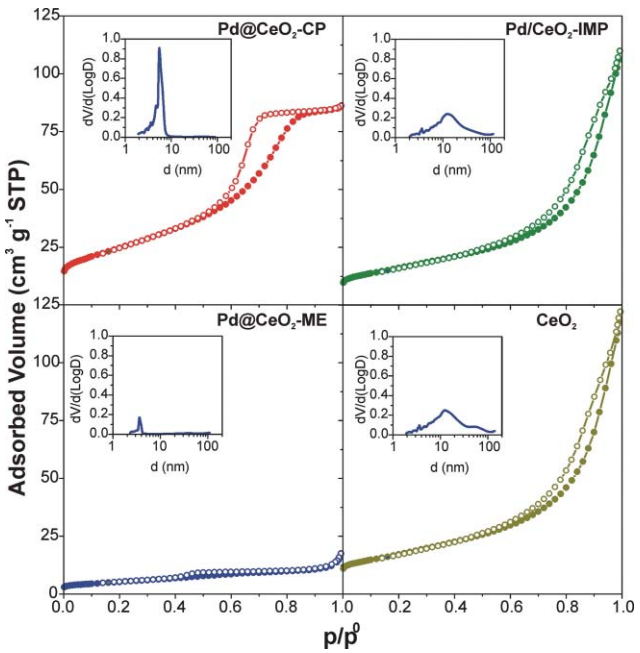

Fig. 1 BET curves of the samples prepared: filled symbols, adsorption branch; empty symbols, desorption branch. The insets show pore distributions.

The Pd@CeO_2-CP sample had the largest specific surface area (80 m^2 g^{-1}) and exhibited a very narrow pore-size distribution. Interestingly, the pore size was peaked at ~5 nm, which is close to the expected size of the core-shell nanoparticles that make up this sample, assuming that the Pd nanoparticles were approximately 1.5 nm and that these were then coated with ceria to form spherical particles with 1-wt% Pd. A CeO_2 sample, which was produced using the same procedure to that used with Pd@CeO_2-CP but without adding Pd nanoparticles, had a lower BET surface area (56 m^2 g^{-1}) and exhibited a much broader range of

Table 1 BET and XRD characterization of the samples prepared

Sample	Surface Area/m^2 g^{-1}	Total Pore Volume/mL g^{-1}	D_{MAX}/nm[a]	CeO_2 crystallite size/nm[b]
Pd@CeO_2-CP	80	0.13	5	10.0
Pd/CeO_2-IMP	56	0.17	12	13.5
Pd@CeO_2-ME	18	0.03	3.5	14.0
CeO_2	56	0.17	12	13.5

[a] Maximum of the pores distribution obtained from the desorption branch. [b] Obtained from CeO_2 (111) reflection in the XRD patterns.

pore sizes. This might suggest that, during the cerium hydroxide formation, the PVP protected Pd particles act as better templating agent than did bare PVP. On the other hand, the Pd/CeO_2-IMP sample had morphological and textural properties almost identical to that of the CeO_2 used to prepare it, showing that the Pd-impregnation and the subsequent calcination steps did not alter the textural properties. Only a slightly different pore size distribution was observed. This is mainly due to the small amount of Pd precursor used to prepare the Pd/CeO_2-IMP sample. In addition, the second lower temperature calcination step (400 °C) used to remove byproducts from the impregnation procedure (*e.g.* nitrates) is unlikely to alter the texture of the CeO_2 support, which had been previously calcined at significantly higher temperature (600 °C). Although materials prepared by hydrolysis of SiO_2 in microemulsions usually have very high surface areas,[21-23] the Pd@CeO_2-ME catalyst had a very low surface area and pore volume. It is possible that fast hydrolysis of the ceric alkoxide leads to a compact distribution of the $Ce(OH)_x$ species around the micelle that then lead to a dense, non porous layer of ceria crystallites around the Pd particles.

TPR profiles of Pd catalysts are reported in Fig. 2. The behaviour of the impregnated catalyst, Pd/CeO_2-IMP, differs remarkably from that of the other two samples. H_2 uptake begins immediately after the temperature is raised from –96 °C to RT. The amount of H_2 taken up in the two RT peaks is approximately 620 μmol H_2/g, a quantity greater than the 94 μmol H_2/g required to reduce Pd from PdO. Some of the additional H_2 uptake is almost certainly due to adsorption of H_2 onto Pd metal; however, most of the H_2 uptake must be associated with reduction of CeO_2 that is in contact with the Pd metal, a result that is consistent with reports in the literature.[24,25] While the presence of two distinct peaks could be due to different chemical processes, the complexities of the transient processes that occur during TPR prevent definitive interpretation of these peaks.[26] Interestingly, the only well-defined feature observed during the temperature ramp on this sample is a small negative peak at ~80 °C that is related to the decomposition of the β-hydride complex.[27,28]

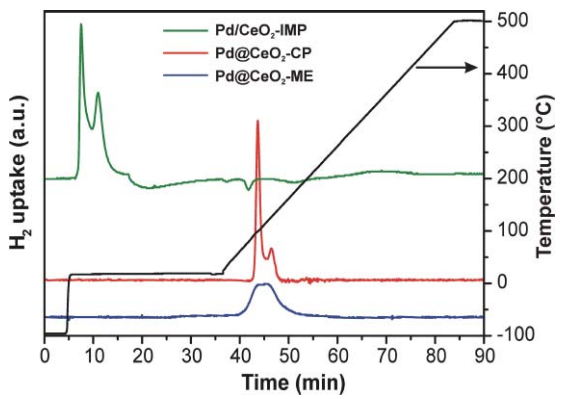

Fig. 2 Temperature Programmed Reduction experiments on Pd-CeO_2 samples.

There was no H_2 uptake observed on the Pd@CeO_2-CP and Pd@CeO_2-ME catalysts at RT; rather, reduction occurred in peaks beginning at ~80 °C on these two samples. While the slight increase in the reduction temperature over that observed on the impregnated sample could be due to the inability of H_2 to access the Pd in the core-shell catalysts,[12,13] the reduction temperatures on these two samples were typical of that observed on other supported Pd catalysts.[29] The amounts of H_2 consumed by these samples, 380 μmol H_2/g on Pd@CeO_2-CP and 400 μmol H_2/g on Pd@CeO_2-ME, were slightly less than that consumed by the impregnated sample, but were still more than the amounts required to reduce the Pd. Interestingly, the Pd@CeO_2-ME sample shows a broader H_2 uptake peak than the Pd@CeO_2-CP sample. This may be an indication that Pd in that sample experiences a broader range of environments (*e.g.* a range of Pd particle sizes).

Table 2 Hydrogen adsorption at –90 °C over Pd-CeO_2 samples after pre-reduction at 200 °C

Sample	H/Pd	Pd surface/m^2 g^{-1} [a]
Pd@CeO_2-CP	0.416	1.85[a]
Pd/CeO_2-IMP	2.490	—
Pd@CeO_2-ME	0.106	0.47[a]

[a] Assuming the formation of surface hydrides only and with a Pd : H = 1 : 1 stoichiometry

In order to characterise the Pd dispersion in these catalysts, H_2 chemisorption experiments were performed at –90 °C, a temperature that has been reported to be sufficiently low so as to avoid spill-over of hydrogen atoms onto the oxide support.[30] These experiments were carried out after the samples had been reduced in H_2 at 200 °C and the results are shown in Table 2. All of the samples exhibited significant H_2 uptakes, showing that some Pd was present at the surface on each of the catalysts. This contrasts with previous reports for Pt@ceria, core-shell catalysts, where the authors believed the Pt was buried by ceria.[12,13] However, the large H_2 uptake on the Pd/CeO_2-IMP sample, corresponding to 2.5 H/Pd, suggests that hydrogen spill-over did occur on this sample at –90 °C. The fact that the hydrogen uptakes were much lower on the Pd@CeO_2-CP sample implies that the Pd is either partially covered or that spill-over is suppressed. The very much lower uptake observed on the Pd@CeO_2-ME sample is likely related to the low specific surface area of that sample, with some Pd buried under ceria layers.

TEM were performed on each of the samples in order to better understand their physical characteristics, with the results shown in Fig. 3. The images clearly show the nanocrystalline structure of CeO_2 in each of the samples but Pd particles could not be identified in any of the micrographs, even though Pd was detected by means of EDX. The Pd@CeO_2-CP and Pd/CeO_2-IMP samples were similar in appearance, which is not surprising given that they were made using the same procedure. In agreement with XRD, the crystallites making up the sample had a characteristic size of approximately 10 nm. While the crystallites that make up the Pd@CeO_2-ME sample were also similar in size, these crystallites appear to be packed more densely, in agreement with conclusions reached from the BET surface areas.

The results from catalytic testing of the three Pd-ceria catalysts are shown in Fig. 4. Fig. 4a shows CO conversion at 250 °C as a function of time for the Pd/CeO_2-IMP sample. The initial conversion was 12% over the first 100 min, implying that this catalyst exhibited a similar activity as observed in a previous study over a 1-wt% Pd/ceria catalyst prepared by impregnation.[14] As observed in the earlier study, exposure of the sample to the WGS

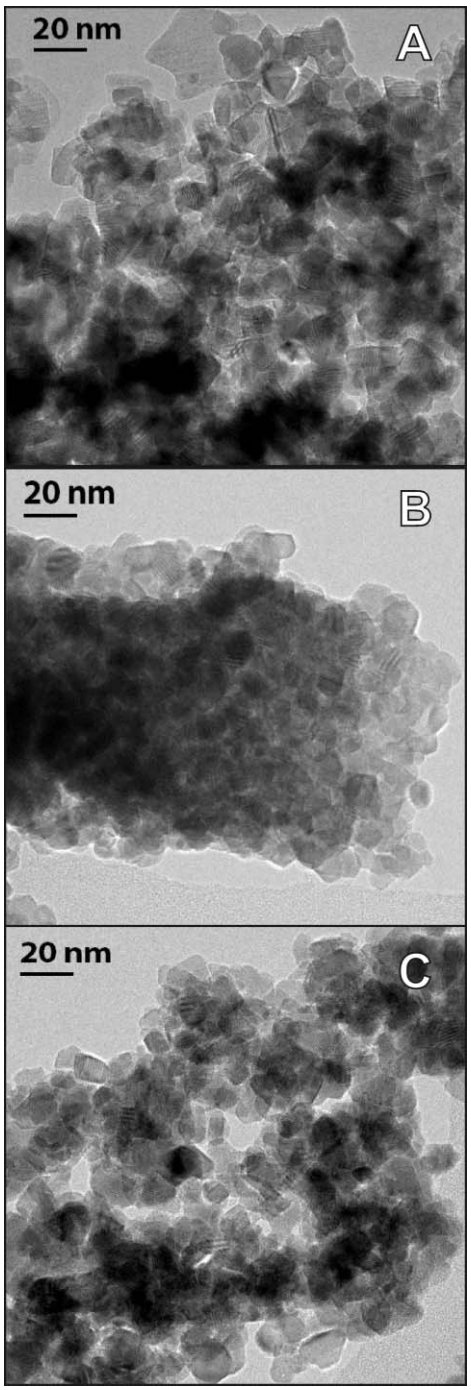

Fig. 3 Representative TEM images of Pd@CeO_2-CP (A), Pd@CeO_2-ME (B) and Pd/CeO_2-IMP (C) catalysts showing nanocrystalline CeO_2.

environment at 400 °C for 3 h caused the conversion at 250 °C to drop significantly, by 25% in this case. The conversion also continued to fall with time. Based on previous studies,[14,15] this deactivation is likely due to a loss of metal dispersion. Oxidation of the sample in a 5% O_2–Ar mixture at 400 °C for 3 h had no effect on the activity, demonstrating that deactivation was likely not due to carbon or carbonate formation. The initial activity was restored following calcination to 600 °C in a 5% O_2–Ar mixture. Since high-temperature oxidation is known to cause redispersion of Pd catalysts,[27] this result is again consistent with the loss of activity

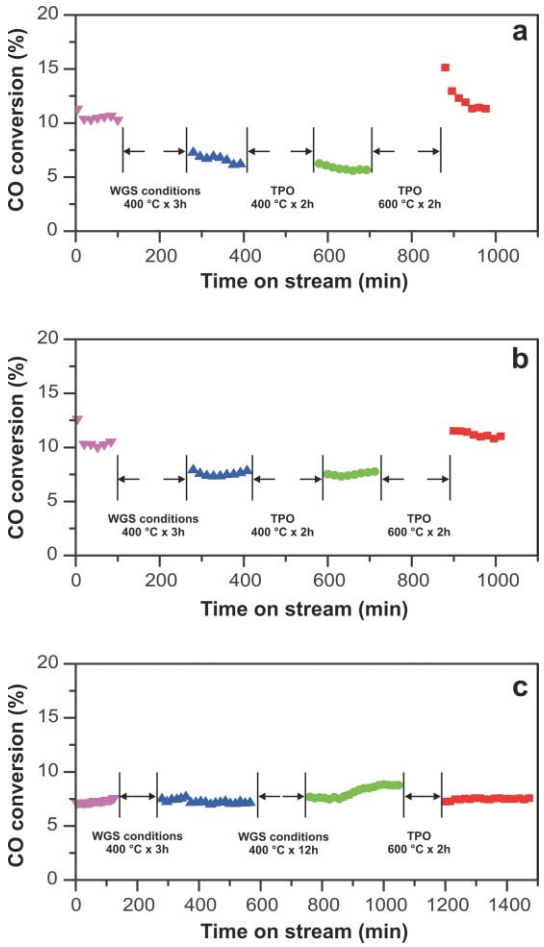

Fig. 4 CO conversions at 250 °C (a,b) and 300 °C (c) under WGSR conditions of Pd/CeO_2-IMP (a), Pd@CeO_2-CP (b) and Pd@CeO_2-ME (c) catalyst after different subsequent treatments.

being due to a loss of metal dispersion. It is important to point out that, even though PdO is almost certainly formed by the oxidative treatments, Pd(II) will also certainly be reduced to Pd(0) in the WGS environment. Therefore, we can exclude the possibility that the increase in the activity following high-temperature calcination is related to a change in the oxidation state of the metal under reaction conditions.

Fig. 4b shows results from the analogous measurements on Pd@CeO_2-CP. The initial activity is almost the same as that observed over Pd/CeO_2-IMP, implying that the metal dispersion must be similar, even though this was not reflected in the H_2 chemisorption results. While exposing the catalyst to the WGS environment at 400 °C resulted in a loss of initial activity, there were no further losses in the catalyst performance at either 250 °C or 400 °C following this treatment. The initial activity was again restored by oxidation at 600 °C. For this sample, we suggest that ceria shell provided some minor enhancement in stability for the Pd particles but that the ceria shell was not sufficiently well formed to completely protect the Pd.

Fig. 4c shows rate data for the Pd@CeO_2-ME sample. The initial activity of this sample was significantly lower, so that rates were measured at 300 °C in order to achieve a similar conversion as that obtained on the other two catalysts. In all likelihood, the lower rate is due to the fact that much of the Pd is not accessible to

the surface, as also shown by the adsorption measurements. What is intriguing about the rate data on this sample is that rates were very stable, even after exposure to the WGS environment at 400 °C for 12 h. Calcination at 600 °C also did not increase the activity of this sample. We suggest that the stability of this sample is due to the trapping of the Pd particles in thicker ceria shells, which then prevented the Pd from sintering. Unfortunately, these same thicker shells also caused the lower initial rates.

Finally, we should point out that the very low concentration of metal in all of the samples and the nature of the samples preclude an accurate investigation of the oxidation state of Pd through spectroscopic means. Although XPS is often used to infer the oxidation state of supported-metal catalysts, charging effects in the presence of non-conductive supports and large peak shifts due to final-state effects associated with small metal particles[31] make determination of this property difficult. Furthermore, the large atomic number for Ce makes the contrast between Pd and ceria poor. However, the highly reducing environment associated with the WGS reaction implies that PdO formed by oxidative treatments (cleaning or TPO) will be readily reduced. Therefore, the differences in catalytic behaviour observed in our studies are almost certainly due to differences in the morphologies of the catalysts and not to differences in the oxidation state of Pd.

While additional work is clearly required, we believe the present results are encouraging in that they appear to demonstrate that the use of core-shell catalysts may allow ceria-supported Pd to be stabilized against sintering for the WGS reaction. Clearly, the "shells" in the present study were not sufficient to achieve the goal: the ceria layer obtained by co-precipitation was not sufficient to prevent sintering of the metal and the ceria layer obtained using microemulsions resulted in materials having a low surface area and with too little of the metal at the surface. Still, as a concept, we believe these materials exhibited sufficient promise for continued developments in this approach.

4. Conclusions

Improvements in stability for the water-gas-shift reaction of $Pd@CeO_2$ over a Pd/CeO_2 catalyst formed by impregnation suggest that the formation of Pd-ceria, core-shell catalysts have great promise for this application. Work is still required to develop core-shell structures that effectively prevent Pd sintering but leave the Pd accessible to gas-phase reactants.

Acknowledgements

The Universities of Trieste and Venice, ICCOM-CNR, INSTM, Fondo Trieste and PRIN2007 "Sustainable processes of 2nd generation for the production of H_2 from renewable resources" are acknowledged for financial support. M. C. thanks the University of Trieste for the PhD fellowship. R. J. G. and N. W. acknowledge support from AFOSR (MURI), Grant No. FA9550-08-1-0309.

Notes and references

1 Y. Piao, Y. Jang, M. Shokouhimehr, I. S. Lee and T. Hyeon, *Small*, 2007, **3**, 255.
2 M. J. Hostetler, J. E. Wingate, C. J. Zhong, J. E. Harris, R. W. Vachet, M. R. Clark, J. D. Londono, S. J. Green, J. J. Stokes, G. D. Wignall, G. L. Glish, M. D. Porter, N. D. Evans and R. W. Murray, *Langmuir*, 1998, **14**, 17.
3 G. Budroni and A. Corma, *Angew. Chem., Int. Ed.*, 2006, **45**, 3328.
4 C. Luo, Y. Zhang and Y. Wang, *J. Mol. Catal. A: Chem.*, 2005, **229**, 7.
5 Z. Li, C. Brouwer and C. He, *Chem. Rev.*, 2008, **108**, 3239.
6 L. De Rogatis, M. Cargnello, V. Gombac, B. Lorenzut, T. Montini and P. Fornasiero, *ChemSusChem*, 2009, DOI: 10.1002/cssc.200900151.
7 S. H. Joo, J. Y. Park, C. K. Tsung, Y. Yamada, P. Yang and G. A. Somorjai, *Nat. Mater.*, 2009, **8**, 126.
8 J. N. Park, A. J. Forman, W. Tang, J. Cheng, Y. S. Hu, H. Lin and E. W. McFarland, *Small*, 2008, **4**, 1694.
9 P. M. Arnal, M. Comotti and F. Schüth, *Angew. Chem., Int. Ed.*, 2006, **45**, 8224.
10 T. Bunluesin, R. J. Gorte and G. W. Graham, *Appl. Catal., B*, 1998, **15**, 107.
11 G. Zhou, P. R. Shah, T. Montini, P. Fornasiero and R. J. Gorte, *Surf. Sci.*, 2007, **601**, 2512.
12 C. M. Y. Yeung and S. C. Tsang, *J. Phys. Chem. C*, 2009, **113**, 6074.
13 C. M. Y. Yeung, K. M. K. Yu, Q. J. Fu, D. Thompsett, M. I. Petch and S. C. Tsang, *J. Am. Chem. Soc.*, 2005, **127**, 18010.
14 X. Wang, R. J. Gorte and J. P. Wagner, *J. Catal.*, 2002, **212**, 225.
15 W. Ruettinger, X. Liu and R. J. Farrauto, *Appl. Catal., B*, 2006, **65**, 135.
16 H. P. Choo, K. Y. Liew and H. Liu, *J. Mater. Chem.*, 2002, **12**, 934.
17 D. Segal, *J. Mater. Chem.*, 1997, **7**, 1297.
18 P. S. Gradeff, F. G. Schreiber, K. C. Brooks and R. E. Sievers, *Inorg. Chem.*, 1985, **24**, 1110.
19 H. Chen, J. A. Cronin and R. D. Archer, *Inorg. Chem.*, 1995, **34**, 2306.
20 P. Fornasiero, R. Di Monte, G. R. Rao, J. Kaspar, S. Meriani, A. Trovarelli and M. Graziani, *J. Catal.*, 1995, **151**, 168.
21 C. Aprile, A. Abad, H. García and A. Corma, *J. Mater. Chem.*, 2005, **15**, 4408.
22 J. Esquena, C. Solans and J. Llorens, *J. Colloid Interface Sci.*, 2000, **225**, 291.
23 T. Hanaoka, M. Kishida, H. Nagata and K. Wakabayashi, *Sekiyu Gakkaishi (Journal of the Japan Petroleum Institute)*, 1996, **39**, 285.
24 H. Zhu, Z. Qin, W. Shan, W. Shen and J. Wang, *J. Catal.*, 2004, **225**, 267.
25 H. W. Jen, G. W. Graham, W. Chun, R. W. McCabe, J. P. Cuif, S. E. Deutsch and O. Touret, *Catal. Today*, 1999, **50**, 309.
26 R. J. Gorte, *Catal. Today*, 1996, **28**, 405.
27 H. Lieske and J. Voelter, *J. Phys. Chem.*, 1985, **89**, 1841.
28 V. Ferrer, A. Moronta, J. Sanchez, R. Solano, S. Bernal and D. Finol, *Catal. Today*, 2005, **107–108**, 487.
29 M. F. Luo, Z. Y. Hou, X. X. Yuan and X. M. Zheng, *Catal. Lett.*, 1998, **50**, 205.
30 J. M. Gatica, R. T. Baker, P. Fornasiero, S. Bernal and J. Kaspar, *J. Phys. Chem. B*, 2001, **105**, 1191.
31 E. I. Altman and R. J. Gorte, *Surf. Sci.*, 1989, **216**, 386.